Experimental demonstration of an entanglement-based quantum router

X.-Y. Chang[1], Y.-X. Wang[1], C. Zu[1], K. Liu[1], L.-M. Duan[1,2]
[1] *Center for Quantum Information, IIIS, Tsinghua University, Beijing, China and*
[2] *Department of Physics, University of Michigan, Ann Arbor, Michigan 48109, USA*

We report an experiment that demonstrates full function of a quantum router using entangled photons, where the paths of a single-photon pulse are controlled in a coherent fashion by polarization of another single photon. Through a projective measurement, we prepare the polarization of the control photon in arbitrary superposition states, leading to coherent routing of the target photon in quantum superposition of different paths. We demonstrate quantum nature of this router through optical measurements based on quantum state tomography and show an average fidelity of $(93.24 \pm 0.23)\,\%$ for the quantum routing operation.

PACS numbers: 03.67.Hk, 03.67.Bg, 42.50.Ex, 03.67.Lx

Quantum network provides the ultimate solution to scalability of quantum computation and communication and has many applications in the context of quantum information science [1, 2]. Similar to a classical network, where routers play an important role for distribution of the signals, quantum routers will be an useful element for building future large-scale quantum network. A router uses a control signal to determine the destination (path) of the data signal. In a quantum network, the data signal is usually carried by a single-photon pulse, which is an ideal carrier of a flying qubit for long-distance communication. One can use a classical router to route quantum information. For instance, an optical switch can efficiently route single-photon pulses [3]. A genuine quantum router, however, offers new possibilities as the control signal itself can be in quantum superposition states. The control signal can be represented by either a photonic or a matter qubit. With the recent advance in technology of high-quality microcavities, one can achieve strong coupling between a trapped matter qubit and the single-photon pulse flying through the cavity **[4]**. Under the strong coupling condition, in principle, a quantum router can be realized if the matter qubit can be controlled in arbitrary superposition states. Such a quantum router induces entangling gates on the incident single-photon pulses, providing an approach for realization of scalable optical quantum computation **[5]**. Experimentally, significant progress has been achieved which demonstrated single-photon routing both in the optical region, where the matter qubit is a single trapped atom **[6]**, and in the microwave region, where the matter qubit is a superconducting transmon **[7]**. However, in the demonstration so far, the matter qubit is prepared only in the classical basis ($|0\rangle$ or $|1\rangle$), and coherence has not been verified yet for a quantum router. To confirm quantum nature of a router, one needs to prepare the matter qubit in superposition states and measure the resulting entanglement between the matter qubit and the photon path. This requires full quantum control of the matter qubit inside the cavity and maintain of coherence for entanglement between the matter qubit and the photon path, which is still experimentally challenging.

In this paper, we take the control qubit as the polarization state of another single photon. It is typically difficult to control the path of a single photon pulse with another single photon as that requires huge nonlinearity not achievable yet in any realistic materials. Instead, in our experiment, we use entangled photons from spontaneous parametric down conversion (SPDC) and linear optical devices to implement the required quantum routing operation. The SPDC setup has proven to be a useful platform for demonstration of quantum information processing **[8, 9],** particularly in connection with the linear optical quantum computation (LOQC) **[10, 11]**. Here, we use this platform to realize the first proof-of-principle demonstration of a genuine quantum router. In this entanglement-based implementation, the control photon is prepared in arbitrary quantum superposition states through a polarizer and wave plates. As the polarizer induces a non-unitary filtering operation, the quantum routing only succeeds with a finite probability (similar to the LOQC experiments [11]). The success is then heralded by the photon detection, and in the event of success, we fully demonstrate quantum nature of the router by showing that it preserves coherence and leads to high-fidelity entanglement between the control qubit and the path of the signal photon. Due to the requirement of prior entanglement and coincidence measurement, similar to many other SPDC experiments, this implementation of the quantum router can not be scaled up to many qubits. However, as a proof-of-principle experiment, it demonstrates for the first time the full quantum nature of the router.

In a quantum router, the polarization of the control qubit can be in arbitrary superposition states $|\Psi_c\rangle = c_0 |H\rangle_c + c_1 |V\rangle_c$, where $|H\rangle_c$ and $|V\rangle_c$ denote two orthogonal linear polarizations. For a signal photon incident from a path denoted by $|L\rangle$, after the router, the final path of this photon is either $|L\rangle_s$ or $|R\rangle_s$, depending on the polarization $|H\rangle$ or $|V\rangle$ of the control qubit. In addition, the coherence between these two possibilities should be maintained, so the final state of the two photons is

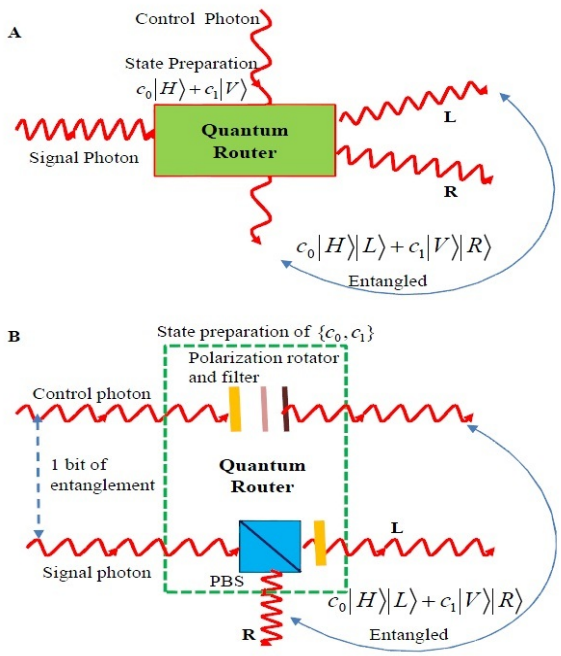

FIG. 1: (A) Illustration of a genuine quantum router. The control photon can be in arbitrary superposition states with coefficients c_0, c_1 that determine the path of the signal photon. The quantum router in general leads to an entangled state $c_0 |H\rangle_c |L\rangle_s + c_1 |V\rangle_c |R\rangle_s$ between the control qubit and the path of the signal photon. (B) The entanglement-based approach to implementation of a genuine quantum router. With a bit of pre-shared entanglement, the quantum router can be realized with linear optical devices. The control coefficients c_0, c_1 are imprinted through operation on the control photon alone with a polarization rotator and a filter. The routing is realized with a polarization beam splitter (PBS) and a wave plate on the signal photon. The setup leads to exactly the same output state $c_0 |H\rangle_c |L\rangle_s + c_1 |V\rangle_c |R\rangle_s$ and realizes the functionality of a quantum router.

given by $|\Psi_f\rangle = c_0 |H\rangle_c |L\rangle_s + c_1 |V\rangle_c |R\rangle_s$. A quantum router thus induces an effective quantum controlled-NOT gate between polarization of the control photon and path of the signal photon as illustrated in Fig. 1A.

In the entanglement-based implementation (see Fig. 1B), we assume that the control photon and the signal photon initially share a bit of entanglement $|\Psi_{cs}\rangle = (|H\rangle_c |H\rangle_s + |V\rangle_c |V\rangle_s)/\sqrt{2}$ in their polarization degrees of freedom. With this pre-shared entanglement, we can then implement the quantum routing through only linear optical devices. The control photon is prepared into the desired state with arbitrary coefficients c_0, c_1 through a combination of polarization rotation and filtering. Without loss of generality, we assume $|c_0| \geq |c_1|$. The polarization filter reduces the V component by a ratio $|c_1/c_0|$ and the wave plates induce a relative phase shift of $\arg(c_1/c_0)$ to the V component. After the control photon passes through the filter (with a success probability of $\left(1 + |c_1/c_0|^2\right)/2$), the effective state between the two photons is described by $|\Psi'_{cs}\rangle = c_0 |H\rangle_c |H\rangle_s + c_1 |V\rangle_c |V\rangle_s$. The signal photon goes through a polarization beam splitter (PBS), which transforms the two photons into a hyper-entangled state $|\Psi_h\rangle = c_0 |H\rangle_c |HL\rangle_s + c_1 |V\rangle_c |VR\rangle_s$ that involves both polarization and path degrees of freedom for the signal photon **[12]**. A half wave plate (HWP) on the L path of the signal photon transforms $|HL\rangle_s \rightarrow |VL\rangle_s$ and factorizes out the polarization degree of freedom $|V\rangle_s$. The final state between polarization of the control photon and path of the signal photon then has the form $|\Psi_f\rangle = c_0 |H\rangle_c |L\rangle_s + c_1 |V\rangle_c |R\rangle_s$. So, with a bit of pre-shared entanglement, the linear optical devices inside the dashed box shown in Fig. 1B gives exactly the quantum routing operation with a success probability of $\left(1 + |c_1/c_0|^2\right)/2$. Note that in this entanglement-based implementation, the coefficients c_0, c_1, which determine the outcome of the quantum router, are still tuned by the operation on the control photon alone.

For experimental demonstration of this entanglement-based approach to a quantum router, we generate the two-photon entangled state $|\Psi_{cs}\rangle$ through the process of spontaneous parametric down conversion. The experimental setup is shown in Fig. 2. We characterize the polarization entanglement in the experimentally generated state ρ through measurements based on the quantum state tomography [14]. For two-qubit states, the quantum state tomography is done with 16 independent measurements in complementary bases and the density matrix is reconstructed using the maximum likelihood method [14]. From the measurements, we find the entanglement fidelity $F \equiv \langle\Psi_{cs}| \rho |\Psi_{cs}\rangle = (96.41 \pm 0.34)\,\%$, where the error bar accounts for the statistical error associated with the photon detection under the assumption of a Poissonian distribution for the photon counts.

With this shared polarization entangled state, the quantum router is realized with the linear optics devices shown in Fig. 2. To verify the quantum routing operation, we prepare the control parameters (c_0, c_1) into six complementary configurations $(1, 0)$, $(0, 1)$, $(1/\sqrt{2}, 1/\sqrt{2})$, $(1/\sqrt{2}, -1/\sqrt{2})$, $(1/\sqrt{2}, i/\sqrt{2})$, $(1/\sqrt{2}, -i/\sqrt{2})$ and measure the fidelity of the output state compared with the ideal case $c_0 |H\rangle_c |L\rangle_s + c_1 |V\rangle_c |R\rangle_s$ for each configuration. To measure the fidelity of the output state, we detect polarization of the control photon and path of the signal photon in several complementary bases. The rotation of the measurement basis for the polarization is achieved with wave plates and a polarizer and for the path is achieved with a Mach-Zehnder interferometer. The control and the signal photons are measured through the single-photon detectors and the outcomes of the detectors are registered through the coincidence circuit.

To verify the quantum routing operation, first we ro-

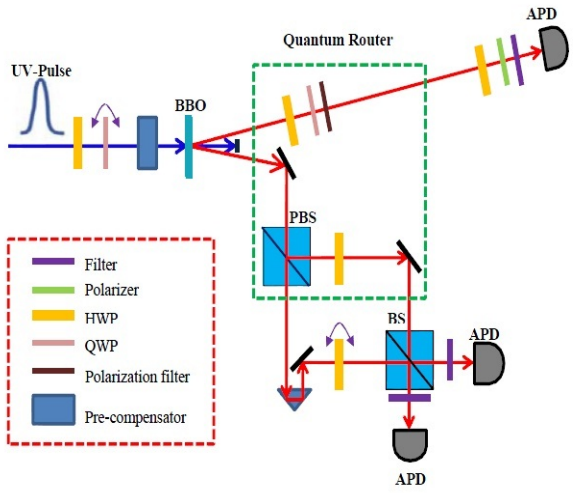

FIG. 2: Experimental setup for realization and verification of the entanglement-based quantum router. To generate entanglement between the control and the signal photons, ultraviolet femtosecond pulses with a repetition rate of 76 MHz from a frequency doubled Ti:sapphire laser pump two joint beta-barium-borate (BBO) crystals, each of 0.6 mm depth with perpendicular optical axis, arranged in the type-I phase matching configuration [**13**]. The pumping pulse is at the wavelength of 400 nm, and its polarization is prepared into the state $(|H\rangle + |V\rangle)/\sqrt{2}$ by controlling a half wave plate (HWP) and a quarter wave plate (QWP) with an adjustable tilting angle. The spontaneous parametric down conversion in two nonlinear crystals generates entangled photon pairs at the wavelength of 800 nm with their polarization described by the state $|\Psi_{cs}\rangle = \left(|H\rangle_c |H\rangle_s + |V\rangle_c |V\rangle_s\right)/\sqrt{2}$. To get a high-fidelity entangled state, a quartz rod of an appropriate length is inserted before the BBO crystals to pre-compensate the temporal walk-off between the polarization components $|H\rangle$ and $|V\rangle$ from birefringence in the BBO crystals. With this shared entangled state $|\Psi_{cs}\rangle$, the linear optical devices inside the dashed box realize the quantum router. The Mach-Zehnder interferometer on the signal photon is used to verify coherence between the two paths. The balance between the two paths is achieved by adjusting a prism, and the relative phase shift on one path is controlled by fine tuning the tilting angle of a HWP. To verify the quantum routing operation, we detect the control and the signal photons in complementary polarization and path bases through the polarization rotator (HWP and QWP) and the Mach-Zehnder interferometer. The single photons are detected with the avalanche photo diodes (APDs). The outcomes of the single-photon detectors are registered through the coincidence circuit. An interference filter of 3 nm bandwidth is inserted before each single-photon detector to filter out the background light and to improve the quality of photonic entanglement.

tate the polarization of the control photon with a polarizer to any state $|\Psi_c(\theta)\rangle = \cos\theta |H\rangle_c + \sin\theta |V\rangle_c$. The path of the signal photon is correspondingly projected to $|\Psi_s\rangle = \cos\theta |L\rangle_s + \sin\theta |V\rangle_s$. In Fig. 3A, we show the photon counts on one path (R) when the polarization of the control photon is projected to $|\Psi_c(\theta)\rangle$. As we vary the polarization angle (θ) of the control photon, the probability for the signal photon going to the path R is well fit with a sine curve with a experimentally measured contrast of 98.7%. We have also measured the probability for the signal photon going to the other path L and found it follows a cosine curve with basically the same contrast.

To confirm that the router maintains quantum coherence, we fix the polarization of the control photon to the state $|\Psi_c(\pi/4)\rangle = (|H\rangle_c + |V\rangle_c)/\sqrt{2}$ and verify the coherence between the two paths of the signal photon. In this case, the signal photon should be in a coherent equal superposition of the L and R paths. We use the Mach-Zehnder interferometer to verify the coherence. The signal photon from the L and the R paths are superposed on a beam splitter (BS) for interference. As the photon pulse has a duration less than 150 fs, we need to use a prism to carefully adjust the interferometer so that it is balanced with equal length for the two arms up to micrometer precision. We then fine tune the relative phase shift ϕ between the two arms by adjusting the titling angle of a quarter wave plate (QWP), which gives a more precise control of ϕ compared with the prism. In Fig. 3B, we show the detector counts on one output of the Mach-Zehnder interferometer as we vary the phase ϕ. It is well fit with a since curve with an experimentally measured contrast of 89.7%, which demonstrates coherence of this quantum router. The imperfection in the contrast is mainly due to the small length fluctuation in the Mach-Zehnder interferometer.

When we take the control parameter (c_0, c_1) as $\left(1/\sqrt{2}, 1/\sqrt{2}\right)$, the output state after the router is a maximally entangled state $|\Psi_f\rangle = (|H\rangle_c |L\rangle_s + |V\rangle_c |R\rangle_s)/\sqrt{2}$ between the polarization of the control photon and the path of the signal photon. We verify this entanglement by reconstructing the density matrix of the output state through measurements based on the quantum state tomography [14]. The real and imaginary parts of all the elements of the density matrix are shown in Fig. 4(A) and 4(B). One can see that the imaginary parts are small and the real parts have good correspondence with the state $|\Psi_f\rangle$. From this measurement, we find that the entanglement fidelity F of the output state is $F = (90.29 \pm 1.56)\%$ and the entanglement measured by the concurrence [15] is $E = 0.8201 \pm 0.0172$. The significant amount of entanglement indicts the quantum nature of this router. The noise is again mainly due to the fluctuation in the Mach-Zehnder interferometer for verification of the entanglement.

We test the performance of the quantum router for the six complementary configurations $(1,0)$, $(0,1)$, $\left(1/\sqrt{2}, \pm 1/\sqrt{2}\right)$, $\left(1/\sqrt{2}, \pm i/\sqrt{2}\right)$ of the control parameters (c_0, c_1), and the fidelities of the output states, compared with the ideal case $c_0 |H\rangle_c |L\rangle_s + c_1 |V\rangle_c |R\rangle_s$, are measured and listed in Table 1. For the first two configurations $(1,0)$, $(0,1)$, the polarization filter in the ex-

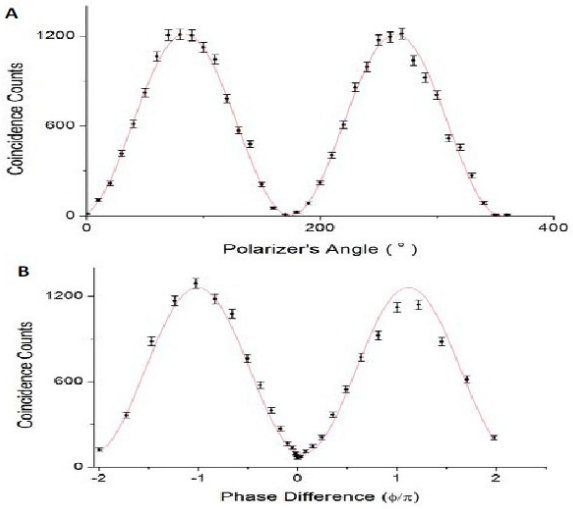

FIG. 3: (A) The photon counts on the path $R$of the signal photon as we vary the polarization angle of the control photon. The dots show the experimental data with error bars accounting for the statistic error from the photon counts. The solid line is a fit with a sine function. (B) The interference from the Mach-Zehnder interferometer as we vary the relative phase shift ϕ of the two paths. The control photon is projected to the state $\left(|H\rangle_c + |V\rangle_c\right)/\sqrt{2}$.

perimental setup shown in Fig. 2 is given by a polarizer. For the other configurations, the filter is actually not necessary. For the four configurations $\left(1/\sqrt{2}, \pm 1/\sqrt{2}\right)$ and $\left(1/\sqrt{2}, \pm i/\sqrt{2}\right)$ that lead to maximally entangled output states, we use a simple inequality derived in Ref. [16] to bound the entanglement fidelity F, which reads $F \geq \left(\rho_{HL} + \rho_{VR} - 2\sqrt{\rho_{HL}\rho_{VR}} + \rho_{++} + \rho_{--} - \rho_{+-} - \rho_{-+}\right)/2$ for the configuration $\left(1/\sqrt{2}, 1/\sqrt{2}\right)$, where $\rho_{\pm\pm}$ denote the matrix elements in the measurement basis $|\pm\rangle$ with $|\pm\rangle = \left(|H\rangle_c \pm |V\rangle_c\right)/\sqrt{2}$ for the control photon and $|\pm\rangle = \left(|L\rangle_s \pm |R\rangle_s\right)/\sqrt{2}$ for the signal photon. Similar inequalities hold for the other configurations with the corresponding change of the measurement basis. The measured lower bounds to these entanglement fidelities are shown in Table 1. For the configuration $\left(1/\sqrt{2}, 1/\sqrt{2}\right)$, this bound is consistent with the fidelity measured through the quantum state tomography. The quantum router induces an effective entangling gate between polarization of the control photon and path of the signal photon. The output state fidelities listed in Table 1 characterize the gate performance under six representative input states. If we average over them, the average gate fidelity is given by $F_g = (93.24 \pm 0.23)\,\%$.

Input parameters (c_0, c_1)	Ideal output state	Fidelity bound
$(1, 0)$	$\|H\rangle_c \|L\rangle_s$	$(98.96 \pm 0.37)\%$
$(0, 1)$	$\|V\rangle_c \|R\rangle_s$	$(97.96 \pm 0.62)\%$
$\left(1/\sqrt{2}, 1/\sqrt{2}\right)$	$\left(\|H\rangle_c \|L\rangle_s + \|V\rangle_c \|R\rangle_s\right)/\sqrt{2}$	$(90.91 \pm 0.55)\%$
$\left(1/\sqrt{2} - 1/\sqrt{2}\right)$	$\left(\|H\rangle_c \|L\rangle_s - \|V\rangle_c \|R\rangle_s\right)/\sqrt{2}$	$(91.20 \pm 0.59)\%$
$\left(1/\sqrt{2}, i/\sqrt{2}\right)$	$\left(\|H\rangle_c \|L\rangle_s + i\|V\rangle_c \|R\rangle_s\right)/\sqrt{2}$	$(90.76 \pm 0.59)\%$
$\left(1/\sqrt{2}, -i/\sqrt{2}\right)$	$\left(\|H\rangle_c \|L\rangle_s - i\|V\rangle_c \|R\rangle_s\right)/\sqrt{2}$	$(89.63 \pm 0.60)\%$

Table 1: List of the measured fidelities (the first two rows) or the lower bounds for the entanglement fidelities (the last four rows) under different configurations of the control parameters (c_0, c_1). The middle column shows the corresponding ideal output states.

In this work, we report a proof-of-principle demonstration of a genuine quantum router with an all optical setup. The quantum nature of the router is demonstrated for the first time through characterization of the resultant entanglement in the output state and the induced effective entangling gate. The quantum router provides a useful element for building future quantum networks.

This work was supported by the National Basic Research Program of China (973 Program) 2011CBA00300 (2011CBA00302) and the NSFC Grant 61033001. LMD acknowledges in addition support from the IARPA MUSIQC program, the ARO and the AFOSR MURI program.

[1] L.-M. Duan and C. Monroe, *Rev. Mod. Phys.* **82**, 1209 (2010).
[2] J. Kim and C. Kim, Quant. Inf. Comput. 9, 2 (2009).
[3] M. A. Hall, J. B. Altepeter, P. Kumar, Phys. Rev. Lett. 106, 053901 (2011); T. Zhang et al., quant-ph/0608238.
[4] K. J. Vahala, *Nature* **424**, 839 (2003).
[5] L.-M. Duan and H. J. Kimble, *Phys. Rev. Lett.* **92**, 127902 (2004).
[6] T. Aoki et al., *Phys. Rev. Lett.* **102**, 083601 (2009).
[7] I.-C. Hoi et al., *Phys. Rev. Lett.* **107**, 073601 (2011).
[8] P. G. Kwiat et al., Phys. Rev. Lett. 75, 4337 (1995).
[9] For a review, see J.-W. Pan et al., arXiv:0805.2853, Rev. Mod. Phys. (to appear).
[10] E. Knill, R. Lafamme, and G. Milburn, Nature (London) 409, 46 (2001).
[11] For a review, see P. Kok et al., Rev. Mod. Phys. 79, 135

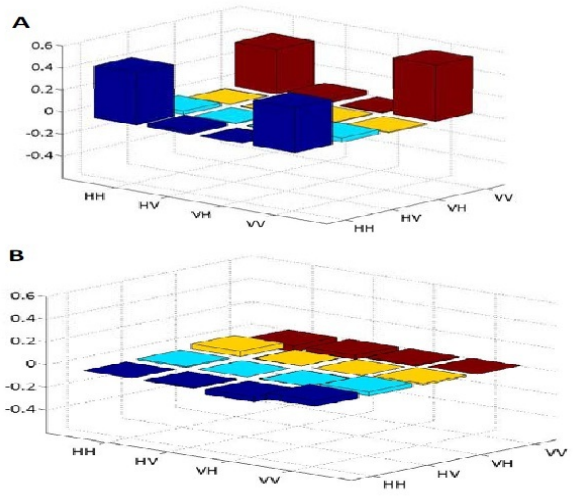

FIG. 4: Real (Fig. A) and Imaginary (B) parts of the density matrix elements of the experimental state reconstructed through the quantum state tomography, describing the entanglement between the polarization of control photon and the path of signal photon. The control parameters (c_0, c_1) are chosen to be $\left(1/\sqrt{2}, 1/\sqrt{2}\right)$.

(2007).
[12] J. T. Barreiro, N. K. Langford, N. A. Peters, P. G. Kwiat, *Phys. Rev. Lett.* **95**, 260501 (2005).
[13] P. G. Kwiat et al., *Phys. Rev. A* **60**, R773-R776 (1999).
[14] D. F. V. James, P. G. Kwiat, W. J. Munro, A. G. White, *Phys. Rev. A* **64**, 052312-052326 (2001).
[15] W. K. Wootters, *Phys. Rev. Lett.* **80**, 2245 (1998).
[16] B. B. Blinov, D. L. Moehring, L.-M. Duan, and C. Monroe, *Nature* **428**, 153 (2004).